ACS Photonics

Letter

pubs.acs.org/journal/apchd5

Thermally Controllable Silicon Photonic Crystal Nanobeam Cavity without Surface Cladding for Sensing Applications

William S. Fegadolli,*[,†] Nicola Pavarelli,[‡] Peter O'Brien,[‡] Samuel Njoroge,[†] Vilson R. Almeida,[§] and Axel Scherer[†]

[†]California Institute of Technology, Pasadena, California, United States

[‡]Tyndall National Institute, University College Cork, Lee Maltings, Cork, Ireland

[§]Instituto Tecnológico de Aeronautica and Instituto de Estudos Avançados, São José dos Campos, Brazil

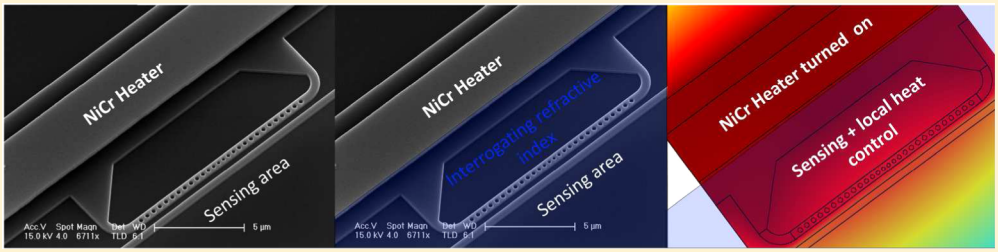

ABSTRACT: Photonic crystal nanobeam cavities with high-quality factors are very sensitive to the dielectric properties of their surroundings. Combining this high sensitivity with a specially designed heater, we experimentally demonstrate a very sensitive optical sensor, capable of simultaneously providing heat and interrogating the refractive index of its surroundings. The structure presents experimental sensitivity of 98 nm/RIU and signal-to-noise ratio of 3.88×10^{-4} RIU and provides approximately 100 °C of temperature variation in the sensing area, with a temperature switching time of a few microseconds.

KEYWORDS: *integrated optics, optical sensing, photonic crystal nanobeam cavity, silicon photonics*

Over the past decades, researchers around the world have focused substantial effort on overcoming the intrinsic limitations of silicon to build integrated optical systems. Building blocks, subsystems, and full systems capable of generating and detecting light by means of hybrid integration of III–V and germanium[1−5] with silicon, as well as CMOS-compatible passive and semiactive devices, enabled this technology to mature to the commercial level and volume production.[6] Because lasers, detectors, passive components, and regular electronics can be monolithically integrated in a single and compact integrated circuit as well as volume produced in well-established foundries across the globe, silicon photonics have become one of the most promising technologies not only for telecommunications but also for sensing applications.

Over the past years, researchers have used the intrinsic compactness and reproducibility of silicon photonics to demonstrate the detection of solid-,[7,8] liquid-,[9,10] and gas-phase materials,[11,12] by using optical resonators and suitable techniques.[7−17] Among the variety of experiments already reported in the literature, two major approaches have been used as sensing mechanisms: refractive index sensing and absorption sensing.[15,16] The refractive index mechanism is based on the detection of a molecular binding-induced refractive index change, near the resonator surface, that is translated to a resonant wavelength shift. The selectivity or specificity of the optical sensor strongly relies on the functionalization performed around the surface of the optical resonator (label detection), which can be achieved by suitable coating or surface preparation processes.[11−16]

These techniques are promising for multiple sensing purposes;[6−18] however, there are longstanding challenges that have limited several bio/chemical sensing applications.[19] One of this challenges consists of the capability of, simultaneously, providing local heat to excite on-chip reactions and optically interrogating the material under analysis. To overcome this challenge, we proposed a specially designed structure, based on a silicon-on-insulator photonic crystal nanobeam cavity, without surface cladding and integrated with a specially designed microheater.

The top view of the proposed structure is schematically shown in Figure 1, which also shows the results of thermal (Figure 1a and its inset) and photonic (Figure 1b) simulations. The structure consists of a silicon photonic crystal nanobeam cavity coupled to a bus waveguide and connected to silicon pads, which are integrated to a NiCr microheater. Since the device has no cladding, the sensor surface corresponds to the immediate surroundings of the tapered region of the nanobeam cavity, where the optical field intensity is stronger.

The entire structure was designed by means of independent photonic and thermal simulations, using tridimensional finite-

Received: December 28, 2014
Published: March 23, 2015

DOI: 10.1021/ph5004863
ACS Photonics 2015, 2, 470−474

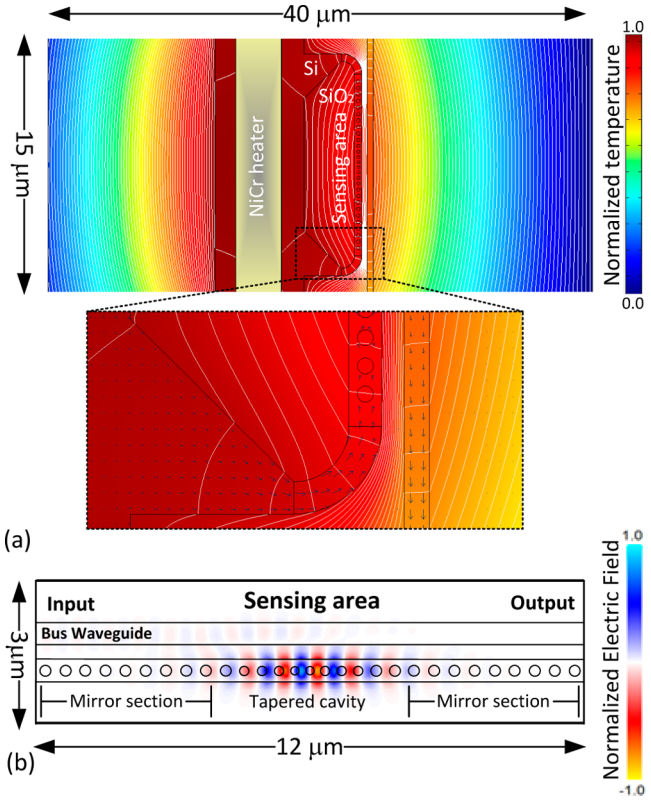

Figure 1. Top view of the proposed structure, which is composed of a photonic crystal nanobeam cavity (waveguide with holes), bus waveguide, and NiCr microheater; the substrate and the ambient (sensing) regions are respectively below and above the figure plane. (a) Theoretical thermal distribution provided by the microheater to the photonic crystal nanobeam cavity. The mapping arrows are normalized regarding the total heat supplied. (b) Theoretical resonant optical mode profile for the photonic crystal nanobeam cavity.

difference time-domain (3D-FDTD) and bidimensional finite element (2D-FE) methods, respectively.

Figure 1a shows thermal simulations of the heat distribution, provided by the 15 μm × 4 μm NiCr microheater on top of the silicon pads. The thermal layer was designed exploiting the principle of thermal conduction; that is, the NiCr heater provides heat to the nanobeam cavity by means of the silicon pads that are connected to its extremities. Evidently, the heat diffuses into both the Si and SiO_2 layers, with a higher level of heat diffusing into the silicon structure due to its higher thermal conductivity, as one can observe in Figure 1a and its inset (the lengths of the mapping arrows are proportional to the total heat supplied).

The heat delivered to the nanobeam cavity increases the refractive index of silicon, by means of its positive thermo-optical coefficient (1.84×10^{-4} K^{-1});[20,21] consequently, the optical length of the cavity increases proportionally, allowing the readout of the temperature based on the tuning of the resonant peak.

The optical design of the proposed structure is composed of the following parameters: the height of the cavity was fixed at 220 nm; the mirror section consists of nine holes with a periodicity of 425 nm and a diameter of 236 nm. The central section of the cavity was precisely tapered within 11 holes, in order to reduce the scattering losses and provide high phase matching between the photonic crystal Bloch mode and the waveguide mode.

The optical simulation results are shown in Figure 1b and Figure 2. Figure 1b shows the theoretical resonant optical mode

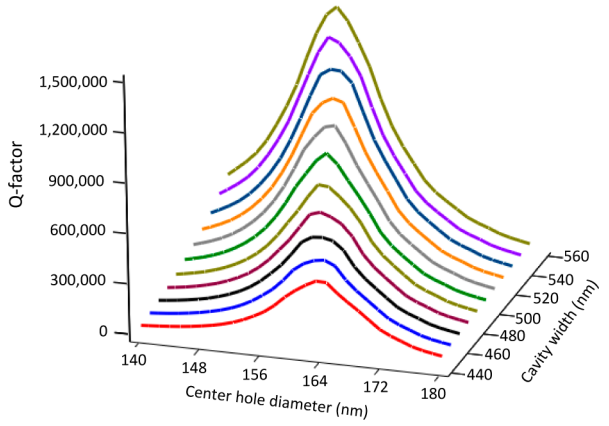

Figure 2. Theoretical unloaded *Q*-factor as a function of the central hole diameter and the cavity width. The *Q*-factor was calculated using the *Q*-finder tool from RSoft Design Group.

of the nanobeam cavity, and Figure 2 shows the behavior of the unloaded (without coupling to the bus waveguide) theoretical *Q*-factor, as a function of the design parameters.

On the basis of Figure 1b, one can see that the optical mode is confined mostly in the central region of the device. Thus, the optical resonant mode is excited by means of the bus waveguide adjacently coupled to the nanobeam cavity. This configuration allows this unique structure to be, simultaneously, optically excited and thermally feed. Thus, owing to its intrinsic nature of being fabricated without surface cladding, it can be used for regular sensing applications,[6−18] as well as for sensing applications that simultaneously require local heating.[19]

The optimized theoretical unloaded *Q*-factor is obtained by choosing a suitable width and diameter of the central hole in the cavity. Figure 2 shows that the theoretical unloaded *Q*-factor of the optimized structure can reach values higher than 1 000 000. However, deviation of a few nanometers in only one of the design parameters can drastically modify the *Q*-factor of the cavity (Figure 2). This demonstrates how challenging the correct fabrication of such structures is.[22]

On the basis of the results of our theoretical investigation and on the resolution of our tunable laser, we selected the cavity width of 510 nm and central hole diameter of 160 nm, which would provide us a theoretical unloaded *Q*-factor of approximately 10^6. However, it is evident that by inserting the bus waveguide coupling, the *Q*-factor is substantially reduced, as a consequence of the loading effect. We also selected a bus waveguide 400 nm wide and 220 nm thick, with a gap separation of 250 nm, in order to provide a reasonable phase matching between the bus waveguide mode and the Bloch mode of the cavity, thus leading to a high extinction ratio of the resonance.

On the basis of this set of design parameters, we fabricated the device with optical and metallic layers. First, the optical layer was exposed by means of electron-beam lithography, using negative tone e-beam resist (XR-1541-HSQ). Subsequently, the sample was developed and then etched by means of a plasma etching, using a mixture of C_4F_8 and SF_6 to define the optical waveguides and the Si pads.

The metallic layer was fabricated by two steps of photolithography, in order to define the microheater and the contact

DOI: 10.1021/ph5004863
ACS Photonics 2015, 2, 470−474

pads. First, the microheater was defined by means of a single aligned step of photolithography, followed by development and deposition of 200 nm of NiCr, and then lift-off. An additional step of aligned photolithography was performed to define the contact pads, followed by developing and two-step deposition of 10 nm of titanium and 270 nm of aluminum, and then lift-off to complete the contact lines.

We performed SiO_2 plasma-enhanced chemical vapor deposition (PECVD) on top of the entire structure and then a last photolithographic step followed by wet etching in order to open a window around the contact pads and also to create a fluid environment around the sensing area, so that its sensing capability could be preserved. It is worthy pointing out that we investigated the deviation in the fabrication process and observed that the diameter of the holes and the width of the cavity, in the fabricated device, accumulate intrinsic and random deviations of up to ±8%.

Finally, the device was packaged using a customized mechanical housing; tapered polarization-maintaining optical fibers were coupled to the silicon chip, and electrical contacts were wire-bonded.

The prototype is shown in Figure 3. Figure 3a and b show scanning electron micrographs, under different magnifications

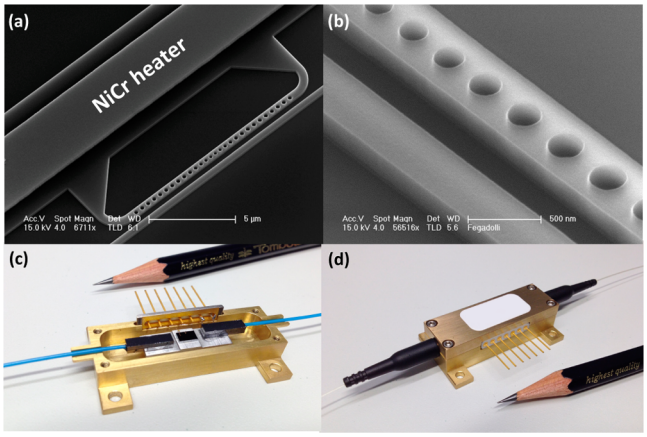

Figure 3. (a, b) Fabricated heater-based photonic crystal nanobeam cavity under different magnifications. (c, d) Different views of the packaged device using edge-coupling design and lensed fibers.

and angles of view, of the fabricated nanobeam cavity integrated with the microheater. Figure 3c and d show two different stages of the packaged device, which employed edge coupling between lensed fibers and nanotapers.[23]

After fabrication, the device was tested using a tunable laser, an electrical pulse generator, and a high-precision multimeter, in order to analyze its figures of merit. Figure 4a shows the device's optical response of the resonator; the maximum extinction ratio observed in our device is 21 dB, for the Quasi-TE_{00} polarization; and the loaded Q-factor is around 20 000. Figure 4b shows the device's optical response for different values of electrical current applied to the microheater.

Additionally, we evaluated the behavior of the resonant shift as a function of the electrical current and power applied on the microheater. Experimental results show that the resistance and electro-optic power efficiency of the device are approximately 130 Ω and 0.015 nm/mW, respectively. The resonant shift as a function of the electrical power and current are shown in Figure 5a.

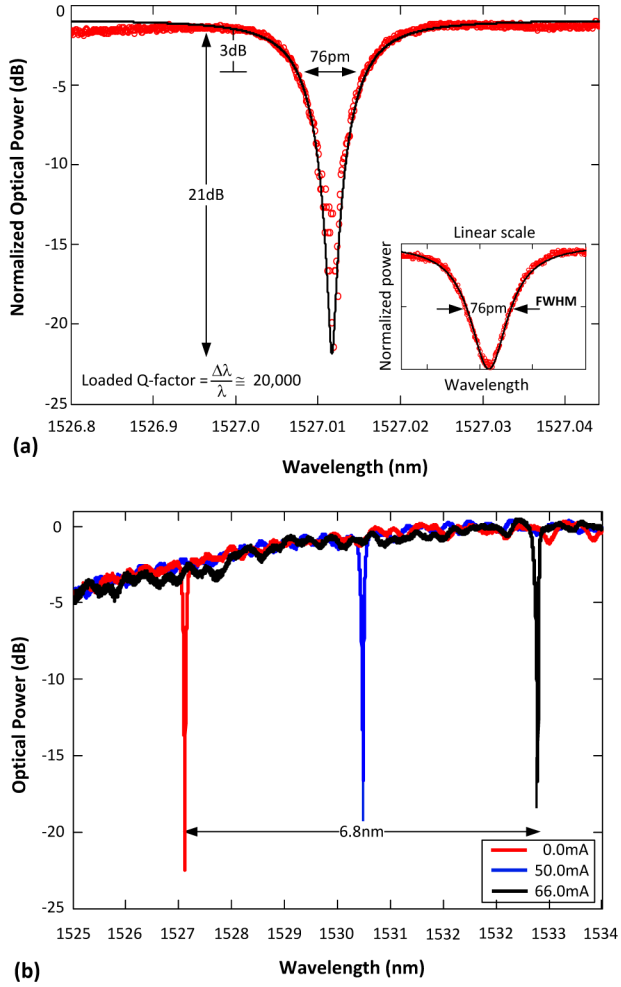

Figure 4. Device's optical response (a) without bias current applied on the microheater and (b) for different electrical current applied on the microheater.

On the basis of our experimental results, it is worthy pointing out that the maximum electrical current applied on the microheater was 66 mA (~566 mW), which causes a maximum resonant shift of up to 6.8 nm. For electrical currents beyond this threshold, we observed physical damage to the microheater.

In order to translate the resonant shift of 6.8 nm in terms of temperature change inside the nanobeam cavity, we have simulated the evolution of the resonant peak as a function of the temperature and found a linear coefficient of approximately 0.07 nm/°C. This allows us to estimate a temperature variation inside the nanobeam cavity of 98 °C before the heater melts down.

We also verified how fast the device is able to switch the resonance; thus, we applied a square electrical signal on the microheater with enough voltage to switch the resonance from *off* to *on* condition. The modulated optical signal was detected by means of a photodetector coupled to an oscilloscope; the results are shown in Figure 5b, where one can observe that the rise and fall times are 10 and 13 μs, respectively;

Furthermore, the sensing capability of our device was characterized by means of detection of four different chemicals using no surface functionalization (label-free detection); a separate sensing device was used for each one of the tests (different chips but same fabrication batch). To perform such an experiment, we introduced the cover medium on each one

DOI: 10.1021/ph5004863
ACS Photonics 2015, 2, 470−474

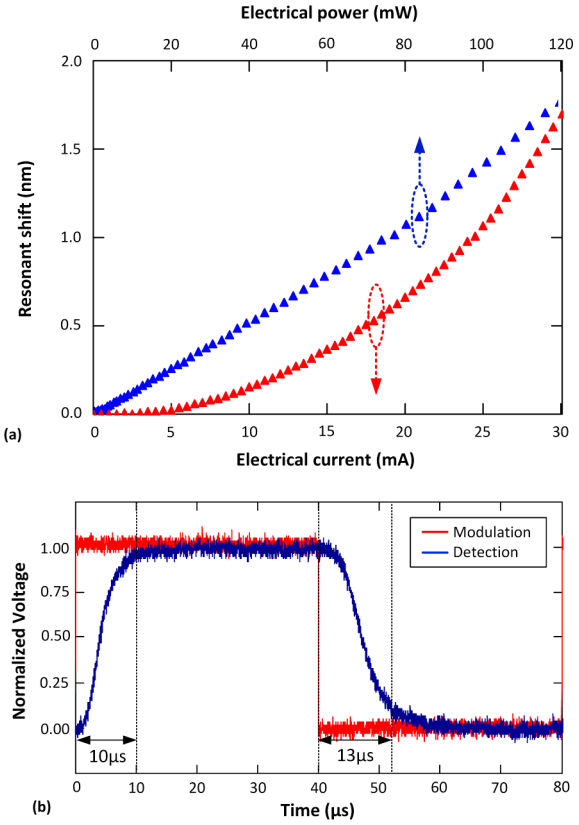

Figure 5. (a) Electro-optical behavior and (b) time response of the fabricated device for the resonant wavelength of 1527.11 nm.

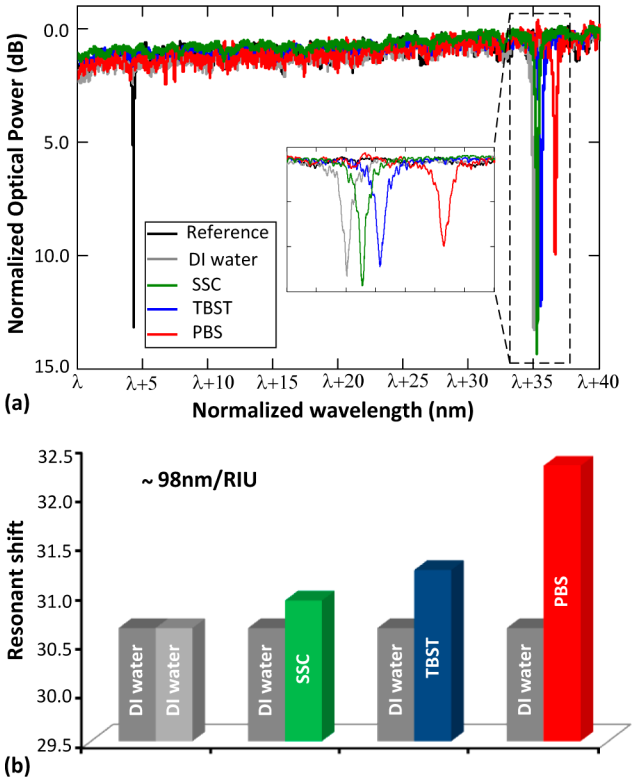

Figure 6. (a) Induced resonant shift for different binding chemistries (inset shows spectral details) and (b) comparison of the resonant shift for different chemicals and DI water.

of our four sensors' surface with deionized water (DI water), saline-sodium citrate (SSC) buffer, Tris-buffered saline and Tween 20 (TBST), and phosphate-buffered saline (PBS), respectively; then we investigated the induced resonant shift caused by the change of refractive index around the surface of the resonator. The results are shown in Figure 6.

It is worth pointing out that a normalized optical wavelength was assumed in Figure 6a, because each one of the optical resonators used in the experiments presented a slightly different resonant wavelength, due to the intrinsic deviations during the fabrication process. Therefore, the single resonant peak, named as reference in Figure 6a, shows a single relative reference resonance that represents the four resonators used in all the experiments.

Figure 6b shows the comparison among the resonant shift of the chemicals used in this experiment and DI water, showing that the device can interrogate chemical signatures of different materials with low refractive index contrast, since all solutions are water based. The experiment was repeated several times with different samples, and no significant discrepancy was observed regarding the resonant wavelength readout.

In order to infer the experimental device's sensitivity, one can consider the DI water refractive index as 1.318[24] and observe the wavelength shift in our experiments, resulting in a sensitivity of approximately 98 nm/RIU, which is consistent with our theoretical results obtained from 3D-FDTD simulations, of about 100 nm/RIU. The smallest refractive index change that can be experimentally detected was conservatively calculated as being 3.88×10^{-4}; this number is found by dividing the resonance resolution, which presents a half-width at half-maximum (HWHM) of 38 pm, by the device sensitivity (of 98 nm/RIU). It is worth pointing out that our device has a theoretical potential to reach Q-factors of up to 1 500 000, which translates into a signal-to-noise ratio several orders of magnitude higher (5×10^{-6}), being comparable to the state-of-the-art refractive index sensors using integrated optics.[11,16,25]

Finally, we have performed a last experiment, joining the capabilities of simultaneously providing heat and interrogating the refractive index near the device's surface. Figure 7 shows the normalized optical power as a function of the wavelength, without any material near the device's surface (reference), with DI water at room temperature, and with DI water plus heat

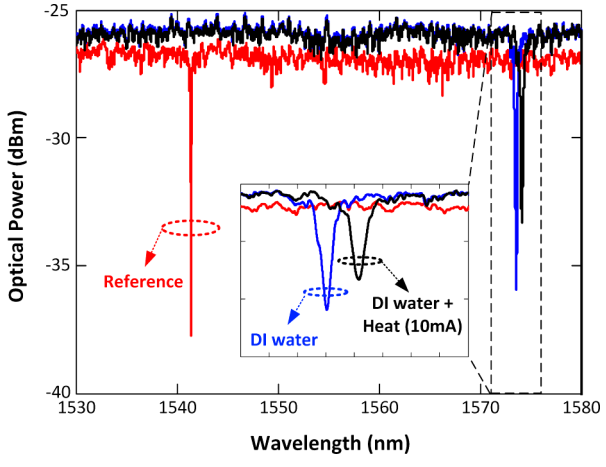

Figure 7. Optical response of the device at different conditions.

DOI: 10.1021/ph5004863
ACS Photonics 2015, 2, 470−474

provided to the resonator, by means of an electrical current of 10 mA.

On the basis of Figure 7, one can observe that the device is able to simultaneously interrogate and heat up materials near the surface of the nanobeam cavity. In addition, it is worth pointing out that we could observe the formation of water bubbles when the heater reached temperatures around 100 °C, by means of an optical microscope placed atop the optical testing setup.

In summary, the results reported in this letter indicate that the proposed structure may offer the potential to achieve, for on-chip scale, the simultaneous capability of interrogation and heat supply, which offers potential applications in biochemical diagnostics that require local temperature control. Such an on-chip capability also offers the potential to develop novel multiplexed sensing techniques for biomedical diagnosis and sensing applications in general, extending the concept shown in this report to a variety of materials in different phases.

AUTHOR INFORMATION

Corresponding Author

*E-mail: fegadoli@caltech.edu.

Notes

The authors declare no competing financial interest.

ACKNOWLEDGMENTS

W.S.F., S.N., and A.S. thank the NSF CIAN ERC (Grant EEC-0812072), Sanofi S. A., and the Gates Foundation for the financial support. V.R.A. thanks CNPq for Grants 483116/2011-4 and 312029/2013-6 and CAPES for the PVS-ITA Grant. N.P. and P.O'B. thank the Irish Photonics Integration Centre (www.ipic.ie) under Science Foundation Ireland (Grant No. 12/RC/2276).

REFERENCES

(1) Liang, D.; Fiorentino, M.; Okumura, T.; Chang, H.-H.; Spencer, D. T.; Kuo, Y.-H.; Fang, A. W.; Dai, D.; Beausoleil, R. G.; Bowers, J. E. Electrically-pumped compact hybrid silicon microring lasers for optical interconnects. *Opt. Express* **2009**, *17*, 20355−20364.

(2) Ohira, K.; Kobayashi, K.; Iizuka, N.; Yoshida, H.; Ezaki, M.; Uemura, H.; Kojima, A.; Nakamura, K.; Furuyama, H.; Shibata, H. On-chip optical interconnection by using integrated III-V laser diode and photodetector with silicon waveguide. *Opt. Express* **2010**, *18*, 15440−15447.

(3) Tanaka, S.; Jeong, S.-H.; Sekiguchi, S.; Kurahashi, T.; Tanaka, Y.; Morito, K. High-output-power, single-wavelength silicon hybrid laser using precise flip-chip bonding technology. *Opt. Express* **2012**, *20*, 28057−28069.

(4) Fegadolli, W. S.; Kim, S.-H.; Postigo, P. A.; Scherer, A. Hybrid single quantum well InP/Si nanobeam lasers for silicon photonics. *Opt. Lett.* **2013**, *38*, 4656−4658.

(5) Creazzo, T.; Marchena, E.; Krasulick, S. B.; Yu, P. K. L.; Orden, D. V.; Spann, J. Y.; Blivin, C. C.; He, L.; Cai, H.; Dallesasse, J. M.; Stone, R. J.; Mizrahi, A. Integrated tunable CMOS laser. *Opt. Express* **2013**, *21*, 28048−28053.

(6) Jalali, B.; Fathpour, S. Silicon photonics. *J. Lightwave Technol.* **2006**, *24*, 4600.

(7) Schmidt, B.; Almeida, V.; Manolatou, C.; Preble, S.; Lipson, M. Nanocavity in a silicon waveguide for ultra sensitive detection. *Appl. Phys. Lett.* **2004**, *85*, 4854−4856.

(8) Lee, M. R.; Fauchet, P. M. Nanoscale microcavity sensor for single particle detection. *Opt. Lett.* **2007**, *32*, 3284−3286.

(9) Zuta, Y.; Goykhman, I.; Desiatov, B.; Levy, U. On-chip switching of a silicon nitride micro-ring resonator based on digital microfluidics platform. *Opt. Express* **2010**, *18*, 24762−24769.

(10) Liu, Y.; Salemink, H. W. M. Photonic crystal-based all-optical on-chip sensor. *Opt. Express* **2012**, *20*, 19912−19920.

(11) Chen, Y.; Fegadolli, W. S.; Jones, W. M.; Scherer, A.; Li, M. Ultrasensitive gas-phase chemical sensing based on functionalized photonic crystal nanobeam cavities. *ACS Nano* **2014**, *8* (1), 522−527.

(12) Robinson, J. T.; Chen, L.; Lipson, M. On-chip gas detection in silicon optical microcavities. *Opt. Express* **2008**, *16*, 4296−4301.

(13) De Vos, K.; Bartolozzi, I.; Schacht, E.; Bienstman, P.; Baets, R. Silicon-on-insulator microring resonator for sensitive and label-free biosensing. *Opt. Express* **2007**, *15*, 7610−7615.

(14) Boyd, R.; Heebner, J. Sensitive disk resonator photonic biosensor. *Appl. Opt.* **2001**, *40*, 5742−5747.

(15) Hu, J.; Sun, X.; Agarwal, A.; Kimerling, L. C. Design guidelines for optical resonator biochemical sensors. *J. Opt. Soc. Am. B* **2009**, *26*, 1032−1041.

(16) Mehrabani, S.; Maker, A. J.; Armani, A. M. Hybrid integrated label-free chemical and biological sensors. *Sensors* **2014**, *14* (4), 5890−5928.

(17) Grist, S. M.; Schmidt, S. A.; Flueckiger, J.; Donzella, V.; Shi, W.; Fard, S. T.; Kirk, J. T.; Ratner, D. M.; Cheung, K. C.; Chrostowski, L. Silicon photonic micro-disk resonators for label-free biosensing. *Opt. Express* **2013**, *21*, 7994−8006.

(18) Zourob, M.; Lakhtakia, A., Eds. *Optical Guided-Wave Chemical and Biosensors I*; Springer: Berlin, 2010.

(19) Bartlett, J. M. S.; Stirling, D. A short history of the polymerase chain reaction. *PCR Protoc.***2003**, 226.

(20) Fegadolli, W. S.; Vargas, G.; Wang, X.; Valini, F.; Barea, L. A. M.; Oliveira, J. E. B.; Frateschi, N.; Scherer, A.; Almeida, V. R.; Panepucci, R. R. Reconfigurable silicon thermo-optical ring resonator switch based on Vernier effect control. *Opt. Express* **2012**, *20*, 14722−14733.

(21) Atabaki, A. H.; Hosseini, E. S.; Eftekhar, A. A.; Yegnanarayanan, S.; Adibi, A. Optimization of metallic microheaters for high-speed reconfigurable silicon photonics. *Opt. Express* **2010**, *18*, 18312−18323.

(22) Deotare, P. B.; McCutcheon, M. W.; Frank, I. W.; Khan, M.; Loncar, M. High quality factor photonic crystal nanobeam cavities. *Appl. Phys. Lett.* **2009**, *94* (12), 121106.

(23) Almeida, V. R.; Panepucci, R. R.; Lipson, M. Nanotaper for compact mode conversion. *Opt. Lett.* **2003**, *28* (15), 1302−1304.

(24) Hale, G. M.; Querry, M. R. Optical constants of water in the 200-nm to 200-μm wavelength region. *Appl. Opt.* **1973**, *12*, 555−563.

(25) Claes, T.; Bogaerts, W.; Bienstman, P. Experimental characterization of a silicon photonic biosensor consisting of two cascaded ring resonators based on the Vernier-effect and introduction of a curve fitting method for an improved detection limit. *Opt. Express* **2010**, *18*, 22747−22761.

DOI: 10.1021/ph5004863
ACS Photonics 2015, 2, 470−474